Eur. J. Mineral., 37, 627–638, 2025
https://doi.org/10.5194/ejm-37-627-2025

European Journal of Mineralogy
Open Access

Vielleaureite-(Ce), a new epidote of the dollaseite group, coexisting with Mn-dominant hellandite in Mn deposits of the central Pyrenees

Alain Ragu[1], Luca Bindi[2], Paola Bonazzi[2,✝], Laurent Remusat[3], and Christian Chopin[4]

[1]Institut des Sciences de la Terre de Paris, Sorbonne Université, 4 place Jussieu, 75005 Paris, France
[2]Dipartimento di Scienze della Terra, Università di Firenze, Via La Pira 4, 50121 Firenze, Italy
[3]Institut de Minéralogie, Physique des Matériaux et Cosmochimie, UMR CNRS 7590, Sorbonne Université, Museum national d'Histoire naturelle, 61 rue Buffon, 75005, Paris, France
[4]Laboratoire de Géologie, ENS – CNRS – PSL, UMR8538, 24 rue Lhomond, 75005 Paris, France
✝deceased

Correspondence: Luca Bindi (luca.bindi@unifi.it) and Christian Chopin (chopin@geologie.ens.fr)

Received: 1 March 2025 – Revised: 30 June 2025 – Accepted: 4 July 2025 – Published: 15 September 2025

Abstract. The new rare-earth element (REE) bearing epidote-supergroup mineral vielleaureite-(Ce), $Mn^{2+}Ce(MgAlMn^{2+})(Si_2O_7)(SiO_4)F(OH)$, is described from a Paleozoic stratiform Mn ore deposit at the Coustou mine above the village of Vielle-Aure, Hautes Pyrénées, France. It occurs as isolated submillimetric prisms in veinlets crosscutting the microcrystalline rhodochrosite ore, associated with rhodochrosite, friedelite, spessartine, "Mn-humite", baryte, and numerous sulfides. The dark-brown "allanite"-looking prisms are patchily zoned from vanadoandrosite-(Ce) or vanadoakasakaite-(Ce) to a near-endmember vielleaureite-(REE) composition, with a strict correlation between F and Mg contents. The empirical formula of the crystal studied is, on an eight-cation basis, $^{A1}(Mn^{2+}_{0.85}Ca_{0.14}Na_{0.01})_{\Sigma 1.00}$ $^{A2}(Ce_{0.66}La_{0.32}Nd_{0.02}Er_{0.01})_{\Sigma 1.00}$ $^{M1}(Mg_{0.71}V_{0.14}Mn^{2+}_{0.08}Mn^{3+}_{0.02}Fe^{3+}_{0.06})_{\Sigma 1.01}$ $^{M2}Al_{1.00}$ $^{M3}(Mn^{2+}_{0.98}Mg_{0.02})_{\Sigma 1.00}$ $^{T}(Si_{2.94}Al_{0.04}B_{0.01})_{\Sigma 2.99}O_{11}(F_{0.85}Cl_{0.01}O_{0.14})_{\Sigma 1.00}$ (OH). The mean refractive index calculated for the holotype composition is $n = 1.79$. The calculated density is $4.33\,g\,cm^{-3}$. Pleochroism is strong: very light yellow < light brown < brown //b. Monoclinic unit-cell parameters refined from single-crystal X-ray diffraction data are $a = 8.8238(13)$ Å, $b = 5.7131(9)$ Å, $c = 10.0034(16)$ Å, $\beta = 112.823(6)°$, $V = 464.80(13)$ Å^3, $Z = 2$. The anisotropic model of the $P2_1/m$ structure converged to 0.0575 for 1565 reflections with $F_o > 4\sigma(F_o)$ and 126 refined parameters; it confirms the Mn^{2+} dominance at the $A1$ and $M3$ sites and the charge compensation of fluorine incorporation at O4 by Mg at $M1$, pointing to a new member of the dollaseite group, the $^{A1}Mn^{2+}$ equivalent of khristovite-(Ce). In the same rocks, "hellandite" was discovered as tiny oriented relict inclusions within vielleaureite-(Ce), locally associated with micrometre-size fluorite and "parisite" inclusions and more rarely as ghost crystals in rhodochrosite. With a Mn/(Mn + Ca) ratio in the range 0.49 to 0.61, this hellandite-group phase is the Mn^{2+} equivalent of hellandite-(Y).

1 Introduction

The Paleozoic stratiform Mn ore deposits in the central Pyrenees have long been known for their metamorphic Mn-silicate assemblages including rhodonite, tephroite, friedelite, and spessartine (Lacroix, 1900). A reinvestigation (Ragu, 1990, 1994; Brugger et al., 1999) revealed the presence of numerous additional, sometimes rare silicate species, such as helvite, hyalophane, humite-group Mn minerals, tinzenite, and welinite and of vanadium-rich phases such as vuorelainenite, MnV_2O_4, nabiasite, $BaMn_9(VO_4)_6(OH)_2$, and the "allanite" described as vanadoandrosite-(Ce), ideally $Mn^{2+}Ce(V^{3+}Al\,Mn^{2+})(Si_2O_7)(SiO_4)O(OH)$, by Cenki-Tok et al. (2006). The study also mentioned the large compositional range of Mn- and rare-earth-element-rich (REE) epidotes[1] in the Pyrenean deposits and drew attention to a chemical trend due to concomitant F and Mg incorporation, as in dollaseite, leading to compositions close to the endmember $Mn^{2+}REE(MgAlMn^{2+})(Si_2O_7)(SiO_4)F(OH)$, which is so far unknown in the dollaseite group of the epidote supergroup. This remained for long the unnamed mineral UM2006-15-SiO:AlFHMgMnREE. Over the years, it proved to be a challenge to find crystals suitable for further characterisation, but this long quest revealed a whole range of Mn-REE-rich epidotes and showed that most samples in which this Mg-F endmember epidote composition was approached also contained Mn-rich to Mn-dominant varieties of the yttrium borosilicate hellandite, ideally $Ca_3(Y,REE)_3AlSi_4B_4O_{22}(OH)_2$.

In the present paper we describe the new dollaseite-group mineral as vielleaureite-(Ce) (IMA no. 2022-134, symbol Vlr-Ce) and document its intriguing textural relations with the hellandite-group phase. Considering the major contributions of our late colleague Paola Bonazzi to the crystal chemistry of the epidote supergroup and the hellandite group, we deemed it appropriate to have this study included in the special issue published in her honour.

2 Geological setting, occurrence

Quoting Cenki-Tok et al. (2006),

> numerous manganese deposits have been mined in the Lower Carboniferous jasper series of the axial zone of the central Pyrenees. The workings form an E–W trending strip about 3 to 4 km wide and 15 km long straddling the Aure and Louron valleys, Hautes Pyrenees, France, about 100 km SW of Toulouse. The series underwent syntectonic regional low-grade low-pressure greenschist-facies metamorphism. It was later intruded by several Late Variscan granite bodies like the Bordères, Néouvielle and Tramesaygues massifs, which crop out less than 5 km to the northeast, northwest and south, respectively, possibly also as undetected cupolas at shallow depth. In the area of interest, the manganese-bearing strata lie 2 to 3 km away from the contact metamorphic aureoles. Quartz, muscovite, chlorite, rare biotite and albite are the main phases in the enclosing schists.

Vielleaureite-(Ce) occurs in Mn-rich lenses interlayered within the siliceous Lower Carboniferous metasediments, specifically in the Aure valley at the Coustou mine above the Vielle-Aure village (Hautes Pyrénées) in millimetre-thick rhodochrosite–sulfide–quartz veinlets cross-cutting the massive microcrystalline rhodochrosite ore. The samples were collected in the Coustou adit, where it crosscuts the Mn-ore, about 10 m from the entrance.

The associated minerals are rhodochrosite, quartz, chalcopyrite, vanadian spessartine (with up to 1.7 wt % F in core), friedelite, androsite-group epidotes, hellandite-(Y) (or a Mn^{2+}-dominant variety, both mostly occurring as relics within the REE-Mn-rich epidotes, as does monazite-(Ce)), baryte, pyrophanite (commonly vanadian), and minor hübnerite, galena, pyrite, ZnS, alabandite, cobaltite, chalcocite, rare skinnerite (?), and locally helvite and welinite; in the carbonate-rich parts, manganhumite also occurs as well as the hellandite phase mentioned above. The enclosing rhodochrosite ore bears fewer sulfides and rhodonite. The mineral formation may be related to fluid circulations through the greenschist-facies metamorphosed Mn-rich sedimentary protolith, probably connected to the intrusion of the nearby (4 km) Néouvielle pluton, dated 302–305 ± 2 Ma (Lemirre et al., 2019).

The new mineral name vielleaureite (/vjɛlˈɔːraɪt/ in the international phonetic alphabet transcription) is for the type locality and is suffixed according to the Levinson (1966) rules for rare-earth-bearing minerals. Note that Lienau (1899) introduced the name viellaurite for one of the local ore types that he considered to be a mineral, but microscopic investigation by Lacroix (1900) of Lienau's samples showed them to be a mixture of rhodochrosite and tephroite. The name has not been used since then and is sufficiently different from vielleaureite-(Ce) to avoid confusion.

The holotype sample (no. VA2016-5) of vielleaureite-(Ce) and the X-rayed crystal have been deposited at the Musée de Minéralogie, Ecole des Mines de Paris, 60 boulevard Saint-Michel, 75006 Paris, France, under catalogue number ENSMP 83943. Cotype material is deposited at the Museum national d'Histoire naturelle, 61 rue Buffon, 75005 Paris, France, catalogue number MNHN_MIN_223.001.

[1] Note that throughout this article the un-suffixed names epidote, allanite, and hellandite, whether singular or plural, are used exclusively in a generic way, i.e. referring to unspecified members of the epidote supergroup and of the allanite and hellandite groups, respectively.

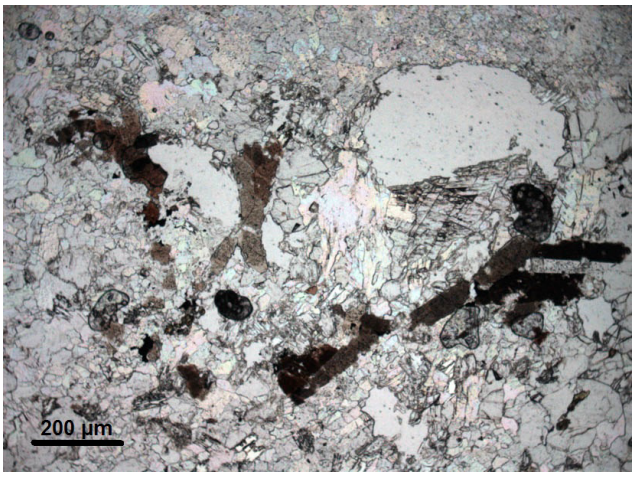

Figure 1. Photomicrograph showing brown prisms of Mn-REE-rich epidote-supergroup minerals (epidotes in the following) in a groundmass of rhodochrosite with friedelite and vanadian spessartine (plane-polarised light, holotype sample VA2016-5). The prisms are chemically patchily zoned, as shown in Figs. 2 to 4. The clear areas are holes, which are artefacts from section preparation.

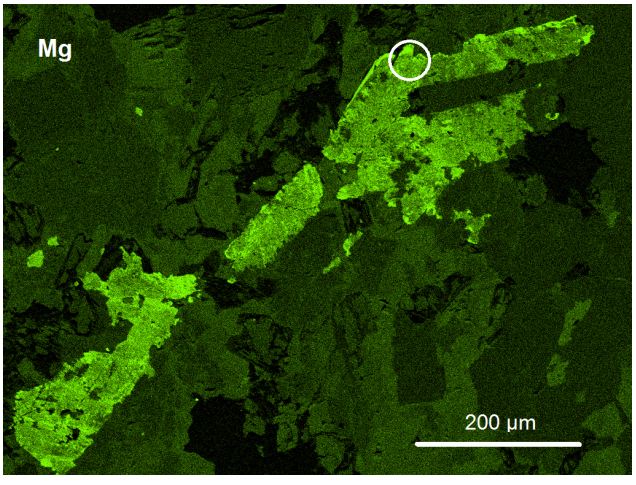

Figure 2. X-ray Mg *K* compositional map of the lower-right part of Fig. 1, showing the heterogeneous distribution of Mg in the epidote prisms (the lighter the shade, the higher the content) and that these, especially in the overgrowths, act as sink for Mg in the rock. The circle indicates the area from which a crystal fragment was extracted for the X-ray work. Holotype sample VA2016-5.

3 Appearance and physical properties

In the samples of interest, allanites occur as scarce dark-brown anhedral to subhedral prismatic grains, elongated along [010] up to 200 µm in size (Fig. 1). Under the electron microscope, they appear compositionally heterogeneous (Fig. 2) – a very common feature in low-metamorphic-grade Mn deposits (e.g. Nagashima et al., 2015; Biagioni et al., 2019; Števko et al., 2023) – with the whole range

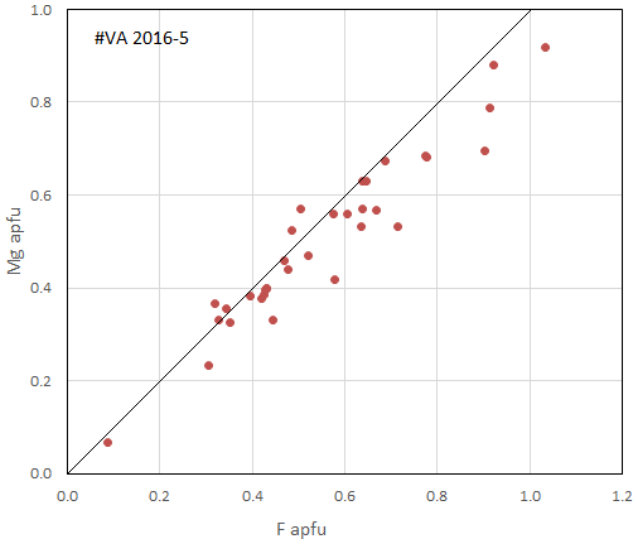

Figure 3. Magnesium content as a function of F content (apfu) in epidotes of holotype sample VA2016-5. It is unclear whether the slight departure from a 1 : 1 Mg : F correlation (shown as a guide) in this batch of electron-microprobe analyses (fluorite standard) results from a slight fluorine overestimation (cf. Fig. 5 in Cenki-Tok et al., 2006, obtained from several other batches of analyses and samples). The divide between the allanite–androsite and dollaseite groups is at F = 0.5 apfu.

of compositions from vanadoandrosite-(Ce) and occasionally vanadoakasakaite-(Ce) (described in between by Nagashima et al., 2024) to near-endmember vielleaureite-(Ce) (as shown below and by Fig. 5 of Cenki-Tok et al., 2006, although the latter was compiled from other samples than the vielleaureite holotype). Near-endmember vielleaureite-(Ce) is consistently found as thin overgrowths (Fig. 2) that are too small for structural work. The mineral is brittle with uneven fractures; neither cleavage nor parting was observed. It is translucent, dark reddish brown, and vitreous to adamantine; the streak is reddish brown. The new mineral is biaxial, $\alpha > 1.74$ (589 nm); the mean refractive index calculated for holotype composition is $n = 1.79$. Pleochroism is strong, very light yellow < light brown < brown //*b*. The high refringence and strong absorption have not allowed further optical characterisation. No fluorescence was observed under the electron beam. The Mohs hardness is likely near 6, by analogy with allanite-group minerals. The calculated density is 4.33 g cm^{-3} on the basis of the empirical formula and unit-cell volume obtained from single-crystal X-ray diffraction (XRD) data (see below).

4 Chemical composition

Electron microprobe (EMP) analyses were obtained in wavelength-dispersive mode using the Cameca SX Five instrument at Camparis, Sorbonne Université, Paris, with

15 kV acceleration voltage (20 kV for hellandite), a 40 nA beam current, and a beam diameter of 2 µm. The standards used were BN (B, $K\alpha$), fluorite or topaz (F, $K\alpha$), albite (Na, $K\alpha$), diopside (Mg and Ca, $K\alpha$), orthoclase (Al, $K\alpha$), almandine (Si, $K\alpha$), apatite (P, $K\alpha$), scapolite (Cl, $K\alpha$), vanadinite (V, $K\alpha$), $MnTiO_3$ (Mn and Ti, $K\alpha$), Fe_2O_3 (Fe, $K\alpha$), $SrSiO_3$ (Sr, $L\alpha$), Y_2O_3 (Y, $L\alpha$), La_3ReO_8 (La, $L\alpha$), monazite (Ce, $L\beta$), Nd_2CuO_4 (Nd, $L\beta$), and Sm_3ReO_8 (Sm, $L\beta$), with REE-bearing glasses for Gd, Dy, Er ($L\beta$), and Yb ($L\alpha$), with due consideration of possible interference and $\phi\rho Z$ data reduction (PAP; Pouchou and Pichoir, 1985).

The small size and heterogeneity of the allanite crystals made it a challenge to characterise the new phase. A fragment extracted from an Mg-rich part of a crystal in a thin section of sample VA2016-5 (Figs. 1 and 2) was finally retained for X-ray work in spite of the poor crystal quality. The mean of four analyses obtained on the area of the crystal relevant to this fragment is given in Table 1 (individual analyses in Table S1 of the Supplement). H_2O was not determined directly because of material paucity and heterogeneity; it was calculated as (OH) = 1.00 atom per formula unit (apfu). The relatively low total is unlikely to be due to incipient metamictisation, given negligible Th and U contents. The resulting empirical formula based on eight cations pfu is

$$^{A1}(Mn^{2+}_{0.85}Ca_{0.14}Na_{0.01})_{\Sigma 1.00}{}^{A2}(Ce_{0.66}La_{0.32}Nd_{0.02}Er_{0.01})_{\Sigma 1.00}$$
$$^{M1}(Mg_{0.71}V_{0.14}Mn^{2+}_{0.08}Mn^{3+}{}_{0.02}Fe^{3+}{}_{0.06})_{\Sigma 1.01}$$
$$^{M2}Al_{1.00}{}^{M3}(Mn^{2+}{}_{0.98}Mg_{0.02})_{\Sigma 1.00}$$
$$^{T1-3}(Si_{2.94}Al_{0.04}B_{0.01})_{\Sigma 2.99}O_{11}(F_{0.85}Cl_{0.01}O_{0.14})_{\Sigma 1.00}(OH),$$

with the Mn^{3+}/Mn^{2+} ratio calculated to ensure electroneutrality.

The simplified formula of vielleaureite-(Ce) is

$$(Mn^{2+}, Ca)(Ce, La)(Mg, V, Mn^{3+}, Fe^{3+})AlMn^{2+}(Si_2O_7)$$
$$(Si, Al)O_4(F, O)(OH);$$

the ideal endmember formula is

$$Mn^{2+}Ce(MgAlMn^{2+})(Si_2O_7)(SiO_4)F(OH).$$

The latter requires (in wt %) SiO_2 29.75, Al_2O_3 8.42, Ce_2O_3 27.10, MnO 23.43, MgO 6.66, F 3.16, H_2O 1.48, sum 100.00.

5 Crystallography

Given the inhomogeneity of the material studied, X-ray powder diffraction data (Table S2 in the Supplement) were collected on the extracted crystal fragment with an Oxford Diffraction Excalibur PX Ultra diffractometer fitted with a 165 mm diagonal Onyx CCD detector and using copper radiation (Cu $K\alpha$, $\lambda = 1.54138$ Å). The unit-cell parameters refined from the powder data in the monoclinic system, space group type $P2_1/m$, are $a = 8.8123(8)$ Å, $b = 5.7108(6)$ Å, $c = 10.0048(13)$ Å, $\beta = 112.810(9)°$, $V = 464.13(6)$ Å^3.

Single-crystal X-ray diffraction intensity data were collected with a Bruker D8 Venture diffractometer equipped with a Photon III CCD detector using Mo$K\alpha$ radiation ($\lambda = 0.71073$ Å). The detector-to-crystal distance was 50 mm. Data were collected using ω and φ scan modes in 0.5° slices, with an exposure time of 20 s per frame. The data were corrected for Lorentz and polarisation factors and for absorption using the software package Apex3 (Bruker AXS Inc., 2016). The unit-cell parameters refined from these data in the monoclinic system, space group type $P2_1/m$, are $a = 8.8238(13)$ Å, $b = 5.7131(9)$ Å, $c = 10.0034(16)$ Å, $\beta = 112.823(6)°$, $V = 464.80(13)$ Å^3, $Z = 2$.

The crystal structure was refined using Shelxl-2014 (Sheldrick, 2015), starting from the atomic coordinates of dollaseite-(Ce) given by Peacor and Dunn (1988). The anisotropic structural model converged to 0.0575 for 1565 reflections, with $F_o > 4\sigma(F_o)$ and 126 refined parameters. Details of the data collection and refinement are given in Table 2. Fractional atom coordinates, site occupancies, and equivalent isotropic displacement parameters are reported in Table 3. Table 4 reports selected bond distances. Table 5 shows the comparison between observed site scattering and that calculated on the basis of the proposed site population. Crystallographic Information Files are provided in the Supplement.

The main structural features of vielleaureite-(Ce) are the same as for other members of the epidote supergroup. Noteworthy, the β angle of 112.8°, the Si1–O9–Si2 angle of 136.2°, and the c parameter of 10.00 Å are the lowest that were measured in the supergroup. These features are shared by members of the androsite group and by khristovite in the dollaseite group; they reflect the chemistry of the phase (see compilations in Nagashima et al., 2015; Biagioni et al., 2019). The a parameter is also one of the shortest of the supergroup, after åskagenite-(Nd). As shown in Table 6, there is a good match between the structural parameters obtained from the X-ray diffraction study (i.e. the average bond distances and the mean electron number per site) and the peculiar chemical composition of the mineral. In particular, the strong preference of the smallest octahedron ($M2$) for Al is confirmed, whereas the occupancy of $M3$ and $M1$, which depend on competing cations, is in keeping with the consolidated rule that implies the largest cation (Mn^{2+} in this case) to be mainly ordered at the largest $M3$ octahedron. Accordingly, $\langle M3\text{–O}\rangle$ (2.197 Å) perfectly matches the value observed in manganiandrosite-(Ce) (Cenki-Tok et al., 2006) for a pure Mn^{2+} population, as also indicated by the mean electron number at the site (24.7). Likewise, the dominance of Mg at the $M1$ octahedron is proven by its mean bond distance (2.004 Å) and mean electron number (15.6).

Finally, the geometrical features of the $A1$ polyhedron ($^{VI}\langle A1\text{–O}\rangle = 2.296$ Å and $\delta_{7-6} = 0.521$ Å; see Bonazzi et al., 1996; Bonazzi and Menchetti, 2004; Nagashima et al.,

Table 1. Chemical data (in wt %) for vielleaureite-(Ce) and the atomic proportions based on eight cations.

Constituent	Mean	Range	e.s.d.	Atom prop.	Probe standard
P_2O_5	0.03	0.00–0.05	0.02	0.00	Apatite ($K\alpha$)
SiO_2	28.08	27.19–28.84	0.85	2.94	Almandine ($K\alpha$)
B_2O_3	0.03	0.00–0.09	0.04	0.01	BN ($K\alpha$)
Al_2O_3	8.44	8.00–8.97	0.43	1.04	Orthoclase ($K\alpha$)
V_2O_3	1.63	0.39–4.00	1.63	0.14	Vanadinite ($K\alpha$)
Fe_2O_3	0.70	0.18–1.73	0.71	0.06	Fe_2O_3 ($K\alpha$)
MnO_{tot}	21.75	19.76–22.73	1.36		$MnTiO_3$ ($K\alpha$)
$Mn_2O_3^*$	0.20			0.02	
MnO*	21.57			1.91	
Y_2O_3	0.04	0.03–0.06	0.01	0.00	Y_2O_3 ($L\alpha$)
La_2O_3	8.36	8.09–9.03	0.45	0.32	La_3ReO_8 ($L\alpha$)
Ce_2O_3	17.23	17.11–17.47	0.16	0.66	Monazite ($L\beta$)
Nd_2O_3	0.57	0.15–0.81	0.29	0.02	Nd_2CuO_4 ($L\beta$)
Sm_2O_3	0.03	0.00–0.07	0.03	0.00	Sm_3ReO_8 ($L\beta$)
Gd_2O_3	0.05	0.00–0.19	0.09	0.00	REE glass 1 ($L\beta$)
Dy_2O_3	0.02	0.00–0.06	0.03	0.00	REE glass 4 ($L\beta$)
Er_2O_3	0.41	0.08–0.77	0.29	0.01	REE glass 4 ($L\beta$)
Yb_2O_3	0.03	0.00–0.12	0.06	0.00	REE glass 2 ($L\alpha$)
MgO	4.71	2.02–5.92	1.83	0.73	Diopside ($K\alpha$)
CaO	1.21	0.57–2.27	0.79	0.14	Diopside ($K\alpha$)
SrO	0.01	0.00–0.03	0.01	0.00	$SrSiO_3$ ($L\alpha$)
Na_2O	0.03	0.00–0.06	0.03	0.00	Albite ($K\alpha$)
F	2.56	0.94–3.38	1.11	0.85	Fluorite ($K\alpha$)
Cl	0.04	0.02–0.06	0.02	0.01	Scapolite ($K\alpha$)
H_2O_{calc}	1.43			1.00	
$-O=F,Cl$	1.08	0.41–1.43	0.46		
Total	96.32				

* Calculated to ensure electroneutrality of the formula.

2015; Biagioni et al., 2019) clearly support the dominance of Mn^{2+} replacing Ca at this site. The bond–valence calculations (Table 6) obtained using the bond–valence parameters of Brese and O'Keeffe (1991) confirm the proposed site population. In particular the bond–valence sum at O4, usually low in epidotes because the O atom at this site acts as an acceptor for the O10–H group, is here very low (1.17 v.u.), confirming the dominance of F^- replacing O^{2-} at the O4 site (yet the O4 label is retained for consistency with earlier epidote studies).

6 Relation to other species

Vielleaureite-(Ce) is a member of the epidote supergroup (Armbruster et al., 2006), in which distinction is mostly made on the basis of cations occupying the large *A* sites and the *M* octahedra. Specifically, with F dominant at the O4 site and Mg dominant at the *M*1 site, it is a member of the dollaseite group, with Mn^{2+} dominant at the *A*1 and *M*3 sites (instead of Ca and Mg, respectively, in dollaseite-(Ce) and instead of Ca and Mn in the ill-characterised khristovite-(Ce); see Table 7 and the discussion in Cenki-Tok et al., 2006). Noteworthy is the recent report of a yet-undescribed endmember epidote from a skarn sample from the Malmkärra iron mines, Norberg, Västmanland (Sweden), which could be the (OH) analogue of dollaseite-(Ce), ideally $CaREE(MgAlMg)(Si_2O_7)(SiO_4)(OH)_2$ (Taddei et al., 2025).

In practice, chemical analysis and/or crystal-structure refinement are necessary for species identification because of the optical similarity of allanites, androsites, and Mn-rich members of the dollaseite group. In the latter, the presence of fluorine (and magnesium) is characteristic (Table 7).

7 Fluorine incorporation

In spite of the extreme Mn richness of these ores, the nearly ideal 1 : 1 correlation between the F and Mg contents pfu in the whole batch of epidote analyses made over the years on Vielle-Aure samples (e.g. Fig. 5 of Cenki-Tok et al., 2006, and Fig. 3 here) is remarkable, implying a strong crystal-chemical control on this substitution. Fluorine incorporation at O4 appears not to be balanced by Mn^{2+} (nor by Fe^{2+}, an unlikely oxidation state here) but exclusively by Mg replacing a trivalent cation in *M*1. As a matter of fact, all members

Table 2. Crystal and experimental data for vielleaureite-(Ce).

Crystal data	
Crystal size (mm)	$0.030 \times 0.025 \times 0.020$
Cell setting, space group	Monoclinic, $P2_1/m$
a (Å)	8.8238(13)
b (Å)	5.7131(9)
c (Å)	10.0034(16)
β (°)	112.823(6)
V (Å^3)	464.80(13)
Z	2
Data collection and refinement	
Radiation, wavelength (Å)	Mo$K\alpha$, 0.71073
Temperature (K)	293
$2\theta_{max}$ (°)	70.24
Measured reflections	16101
Unique reflections	2224
Reflections with $F_o > 4\sigma(F_o)$	1565
R_{int}	0.0747
$R\sigma$	0.1036
Range of h, k, l	$-14 \le h \le 12, -9 \le k \le 8, -14 \le l \le 16$
$R[F_o > 4\sigma(F_o)]$	0.0575
R (all data)	0.1002
wR (on F_o^2)	0.1168
GoF	1.028
Number of least-squares parameters	126
Maximum and	1.90 (at 1.09 Å from O7)
minimum residual peak (e Å^{-3})	−2.51 (at 0.69 Å from $A2$)

Table 3. Sites, site occupancies (s.o.), fractional atom coordinates, and isotropic (*) or equivalent isotropic displacement parameters (in Å^2) for vielleaureite-(Ce).

Site	s.o.	x	y	z	U_{eq}
$A1$	$Mn_{0.75(3)}Ca_{0.25}$	0.7637(2)	3/4	0.15423(17)	0.0173(4)
$A2$	$Ce_{0.967(8)}Ca_{0.033}$	0.59257(7)	3/4	0.42900(6)	0.01574(17)
$M1$	$Al_{0.688(14)}Mn_{0.312}$	0	0	0	0.0143(6)
$M2$	$Al_{1.00}$	0	0	0.5	0.0125(5)
$M3$	$Mn_{0.975(16)}Al_{0.025}$	0.31964(18)	1/4	0.20396(16)	0.0165(4)
Si1	$Si_{1.00}$	0.3491(3)	3/4	0.0322(3)	0.0135(5)
Si2	$Si_{1.00}$	0.6960(3)	1/4	0.2844(3)	0.0131(5)
Si3	$Si_{1.00}$	0.1904(3)	3/4	0.3215(3)	0.0118(5)
O1	$O_{1.00}$	0.2421(6)	0.9907(8)	0.0197(5)	0.0161(9)
O2	$O_{1.00}$	0.3151(5)	0.9744(8)	0.3587(5)	0.0144(9)
O3	$O_{1.00}$	0.8074(6)	0.0112(8)	0.3304(5)	0.0161(9)
O4	$O_{1.00}$	0.0559(8)	1/4	0.1374(8)	0.0175(13)
O5	$O_{1.00}$	0.0487(8)	3/4	0.1557(7)	0.0151(12)
O6	$O_{1.00}$	0.0818(8)	3/4	0.4216(7)	0.0136(11)
O7	$O_{1.00}$	0.5152(9)	3/4	0.1736(8)	0.0191(14)
O8	$O_{1.00}$	0.5615(8)	1/4	0.3536(7)	0.0202(14)
O9	$O_{1.00}$	0.5988(8)	1/4	0.1071(7)	0.0195(14)
O10	$O_{1.00}$	0.093 (11)	1/4	0.4333(10)	0.0160(13)
H10	$H_{1.00}$	0.07(3)	1/4	0.39(3)	0.11(11)*

Table 4. Selected bond distances (in Å) in vielleaureite-(Ce).

*A*1	–O7	2.275(7)	*A*2	–O7	2.375(7)	*M*1	–O4	1.910(5) × 2	*M*2	–O3	1.880(5) × 2
	–O3	2.226(5) × 2		–O2	2.512(4) × 2		–O5	2.032(5) × 2		–O10	1.897(5) × 2
	–O1	2.270(5) × 2		–O10	2.569(9)		–O1	2.069(4) × 2		–O6	1.901(4) × 2
	–O5	2.509(7)		–O2	2.607(4) × 2	⟨*M*1–O⟩		2.004	⟨*M*2–O⟩		1.893
	–O6	3.030(7)		–O3	2.871(5) × 2						
⟨*A*1–O⟩		2.401		–O8	2.940(5) × 2						
			⟨*A*2–O⟩		2.680						
*M*3	–O8	2.078(7)	Si1	–O7	1.594(8)	Si2	–O8	1.589(7)	Si3	–O2	1.636(5) × 2
	–O4	2.158(7)		–O9	1.629(7)		–O3	1.639(5) × 2		–O6	1.633(7)
	–O2	2.219(5) × 2		–O1	1.645(5) × 2		–O9	1.644(7)		–O5	1.645(7)
	–O1	2.255(5) × 2	⟨Si1–O⟩		1.628	⟨Si2–O⟩		1.628	⟨Si3–O⟩		1.638
⟨M3–O⟩		2.197									

Table 5. Refined site scattering vs. calculated site scattering (in electrons) and site population at the *A* and *M* sites.

Site	Refined site scattering	Proposed site population	Calculated site scattering
*A*1	23.8	$Mn^{2+}_{0.85}Ca_{0.14}Na_{0.01}$	24.2
*A*2	56.8	$Ce_{0.66}La_{0.32}Nd_{0.02}$	57.7
*M*1	16.7	$Mg_{0.71}V_{0.14}Mn_{0.09}Fe^{3+}_{0.06}$	15.6
*M*2	13.0	$Al_{1.00}$	13.0
*M*3	24.7	$Mn^{2+}_{0.98}Mg_{0.02}$	24.7

of the dollaseite group do have Mg as a cation in *M*1, charge compensating the presence of fluorine at O4. Even in Fe-rich systems, F incorporation in epidote is strictly coupled with Mg incorporation (e.g. Fig. 17 in Holtstam and Andersson, 2007; Fig. 4 in Števko et al., 2023); this also holds true for the epidote E module in members of the gatelite supergroup (Bonazzi et al., 2019) – e.g. F incorporation in ferriperbøeite-(Ce) (with ferriallanite E module; Bindi et al., 2018) leads to västmanlandite-(Ce), with dollaseite E module (Holtstam et al., 2005, their Fig. 2), i.e. the $^{M1}Fe^{3+}\ ^{M3}Fe^{2+}\ O4 = {}^{M1}Mg\ {}^{M3}Mg\ F$ substitution.

Figure 4 shows the contents of non-tetrahedral cations as a function of F content in epidotes of holotype sample VA2016-5. It shows how the chemistry of the phase refines with increasing F (i.e. becomes less and less "promiscuous") to end up with the Ca–Fe–V–free vielleaureite endmember. The substitution scheme is $^{M1}Me^{3+} + {}^{O4}O^{2-} = {}^{M1}Mg^{2+} + {}^{O4}F^{-}$, where Me stands for V, Fe, and Al.

The near-origin intercept of the Mg vs. F correlation in our allanite analyses (Figs. 3 and 4) implies the absence of a dissakisite component in all of them. Clearly, in such very Mn-rich rocks, Mg can only be incorporated along with F in allanites. The F-bearing allanites do incorporate Mg and not Mn for charge balance and then paradoxically act as a Mg sink in the rock (see Fig. 2) – to the extent that F and REEs are available.

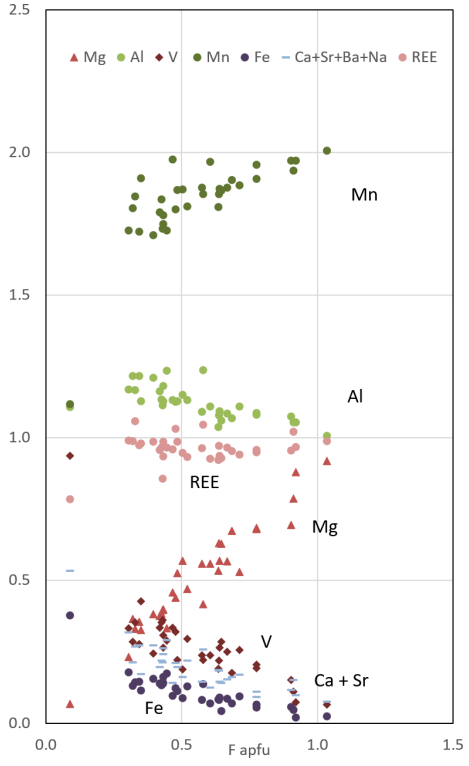

Figure 4. Contents of non-tetrahedral cations as a function of F content (apfu) in epidotes of holotype sample VA2016-5. With increasing F content, Mg replaces V, Fe, and to some extent Al (in the *M* sites), and, accessorily, Mn replaces the minor Ca contents (in the *A*1 site). As a result, the mineral composition evolves from dominant vanadoandrosite to endmember vielleaureite (2Mn : 1REE : 1Al : 1Mg stoichiometry), with the divide at F = 0.5 apfu.

8 Origin and associated minerals

8.1 Fluorine source, textural relations

In a search for clues to possible reactants to form vielleaureite-(Ce), scanning electron microscopy revealed the discrete presence of a number of phases new to these

Table 6. Bond–valence balance (in v.u.) in vielleaureite-(Ce), calculated with the site populations given in Table 5.

	*A*1	*A*2	*M*1	*M*2	*M*3	Si1	Si2	Si3	Σanions
O1	$0.30^{\downarrow\times2}$		$0.38^{\downarrow\times2}$		$0.28^{\downarrow\times2}$	$0.98^{\downarrow\times2}$			1.94
O2		$0.39^{\downarrow\times2}$			$0.31^{\downarrow\times2}$			$1.01^{\downarrow\times2}$	2.01
		$0.30^{\downarrow\times2}$							
O3	$0.34^{\downarrow\times2}$	$0.15^{\downarrow\times2}$		$0.50^{\downarrow\times2}$			$1.00^{\downarrow\times2}$		1.99
O4*			$^{2x\rightarrow}0.44^{\downarrow\times2}$		0.29				1.17
O5	0.16		$^{2x\rightarrow}0.42^{\downarrow\times2}$					0.99	1.99
O6	0.04			$^{2x\rightarrow}0.47^{\downarrow\times2}$				1.02	2.00
O7	0.30	0.57				1.13			2.00
O8		$^{2x\rightarrow}0.12^{\downarrow\times2}$			0.46		1.15		1.85
O9						1.03	0.99		2.02
O10		0.34		$^{2x\rightarrow}0.47^{\downarrow\times2}$					1.28
Σcations	1.78	2.83	2.48	2.88	1.93	4.12	4.14	4.03	
Theor.	1.99	3.00	2.29	3.00	2.00				

Note that left and right superscripts indicate the number of equivalent bonds involving anions and cations, respectively. For sites with mixed occupancy, the bond valences have been weighted.
O4 was considered to be $F_{0.75}O_{0.25}$.

Table 7. Ideal site population of some relevant species of the allanite and dollaseite groups in the epidote supergroup.

Mineral/site	*A*1	*A*2	*M*1	*M*2	*M*3	O4	Reference
Uedaite-(Ce)	Mn^{2+}	Ce	Al	Al	Fe^{2+}	O	Miyawaki et al. (2008)
Ferriakasakaite-(Ce)	Ca	Ce	Fe^{3+}	Al	Mn^{2+}	O	Biagioni et al. (2019)
Ferriandrosite-(Ce)	Mn^{2+}	Ce	Fe^{3+}	Al	Mn^{2+}	O	Števko et al. (2023)
Manganiandrosite-(Ce)	Mn^{2+}	Ce	Mn^{3+}	Al	Mn^{2+}	O	Cenki-Tok et al. (2006)
Vanadoandrosite-(Ce)	Mn^{2+}	Ce	V^{3+}	Al	Mn^{2+}	O	Cenki-Tok et al. (2006)
Dissakisite-(Ce)	Ca	Ce	Al	Al	Mg	O	Grew et al. (1991)
Dollaseite-(Ce)	Ca	Ce	Mg	Al	Mg	F	Peacor and Dunn (1988)
Khristovite-(Ce)	Ca	Ce	Mg	Al	Mn^{2+}	F	Pautov et al. (1993)
Vielleaureite-(Ce)	Mn^{2+}	Ce	Mg	Al	Mn^{2+}	F	This study

Pyrenean deposits and apparently restricted to allanite-bearing samples, especially those in which allanites have a large or dominant vielleaureite component. These phases are REE-fluorocarbonate, fluorides, and an Al-silicate with hellandite-(Y) stoichiometry but Mn ≥ Ca. The REE-fluorocarbonate ("parisite") occurs consistently as tiny relics included in vielleaureite-(Ce)/vanadoandrosite-(Ce) crystals (as observed in samples VAIN86, VA2018-4, VA2018-10), which is occasionally associated with an unidentified Y-silicate (VA2018-10, Fig. 5). Fluorides are a unique micrometre-size grain of BaFCl, likely zhangpeishanite included in vanadoandrosite (VA2018-11), and fluorite in a micrometric intergrowth with hellandite included in and apparently corroded by vielleaureite-(Ce) (VAIN86, Fig. 6a–b). These F-carrier phases do not occur in the matrix but only as inclusions shielded by allanite or by hellandite within allanite; they are therefore armoured relics of reactants that may have acted as fluorine sources during the growth of the vanadoandrosite-(Ce)/vielleaureite-(Ce) crystals.

The textural status of hellandite is more ambiguous. It mostly occurs as tiny corroded inclusions in allanite (revealed by a slightly brighter shade on backscattered electron images; Fig. 7a–d) that occasionally shares the same elongation as the host crystal (Figs. 6a–b, 7b) and so appears as a relict phase. One somewhat-larger crystal was observed in the matrix, but it is also partly overgrown by vielleaureite (Fig. 7a, lower-left corner). However, other rare hellandite crystals do occur in the matrix; they are mostly "ghost" skeletal crystals in rhodochrosite, which may themselves be partly overgrown and included in allanite without the carbonate (Fig. 7d). In the absence of suitable material for X-ray diffraction studies, a preliminary electron backscatter diffraction (EBSD) investigation (details in the Supplement) confirmed two points: (i) importantly, the "hellandite" phase does have the symmetry and structure type of hellandite-(Y) and (ii) the oriented hellandite inclusions are generally part of a single crystal, but no consistent crystallographic relationships with the host allanite were found (the two structures admittedly have little in common). Hellandite may there-

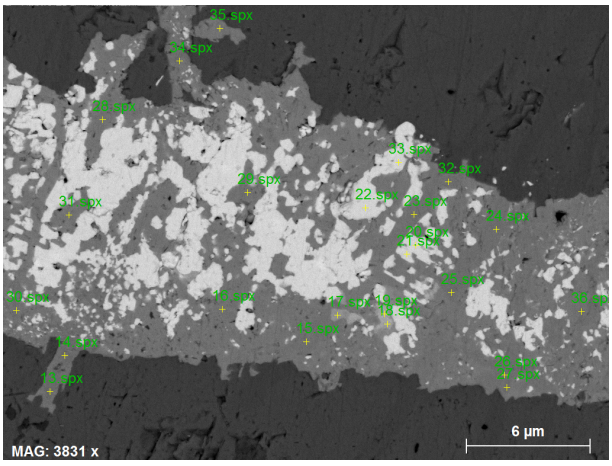

Figure 5. Inclusions of parisite-(La) (large bright speckles) in an epidote prism (medium grey); they are associated with a few tiny grains of an unidentified Y-silicate (intermediate grey shade, e.g. spots 17 to 19). Rhodochrosite matrix (dark-grey shade), BSE image, sample VA2018-10.

fore be a relatively early phase, which then coexisted with vanadoandrosite/vielleaureite but was corroded and (incompletely) consumed at the same time. A closer look at its actual composition may shed some light on possible phase relations with the allanites.

8.2 Mn-dominant hellandite

The small size of the hellandite crystals was not the only challenge for EMP analysis. This analysis confirmed the general dominance of Mn over Ca, with Mn/(Ca + Mn) atomic ratios in the range of 0.49 to 0.61, but the boron values (obtained with a BN standard and PC2 dispersing crystal) are rather dispersed and overestimated (Table 8) with respect to the ideal B_4Si_4 stoichiometry, a problem already encountered by Miyawaki et al. (2015). Significantly, the B contents we measured during the same session for tinzenite from a nearby locality ($Ca_2Mn_4Al_4[B_2Si_8O_{30}](OH)_2$; Grew, 2018) were very close to stoichiometric values, suggesting that the problem may lie in the absorption correction, which could be inappropriate for the heavy matrix of hellandite. In an attempt to clarify the point and because the hellandite structure can host major Li or Be (Oberti et al., 2002, 2019), light elements were analysed by NanoSIMS (details in the Supplement). The Li and Be contents appeared to be at the trace level (Li counts as low as the nominally Li-free quartz standard; Be/Si = 0.0096(6)); the B/Si ratio of 0.98(8) is indeed stoichiometric, and the OH/Si ratio of 0.56(7) is nearly so. Hellandite formulae were therefore calculated on a four-Si basis, assuming stoichiometric B content (Table 8).

The formula resulting from the mean of five analyses is, with Ln = lanthanides, $(Mn^{2+}_{1.76}Ca_{1.41})_{\Sigma 3.17}(Y_{1.37}Ln_{1.45})_{\Sigma 2.82}(Al_{0.83}V^{3+}_{0.10}Mg_{0.04})_{\Sigma 0.97}Be_{0.04}B_4Si_4O_{22}(OH_{1.97}F_{0.03})_{\Sigma 2}$, in which the deficit of 0.23 positive charge can be compensated for assuming 0.23 Mn to be Mn^{3+} or 0.23 additional protons. Given the hellandite struc-

Table 8. Mn-rich hellandite: EMP analyses and formulae (Si = 4 basis).

Sample	VAIN86				VAIN86b	Mean
SiO_2	21.26	22.01	21.05	22.49	21.80	21.72
$B_2O_3^*$	14.97	14.59	14.71	12.29	14.53	12.58
Al_2O_3	3.66	4.03	3.68	4.31	3.51	3.84
TiO_2	0.01	0.01	0.01	0.00	0.00	0.01
V_2O_3	0.63	0.67	0.46	0.65	0.97	0.67
Fe_2O_3	0.00	0.00	0.00	0.00	0.00	0.00
BeO*						0.09
MgO	0.00	0.36	0.00	0.42	0.00	0.16
CaO	7.48	6.29	7.59	6.59	7.70	7.13
MnO	10.44	12.33	10.38	12.55	10.84	11.31
SrO	0.00	0.00	0.00	0.00	0.00	0.00
Y_2O_3	13.77	15.61	13.34	13.17	13.80	13.94
La_2O_3	0.17	0.25	0.00	0.12	0.10	0.13
Ce_2O_3	2.14	2.46	3.03	3.13	2.15	2.58
Pr_2O_3	0.60	0.47	0.33	0.39	0.70	0.50
Nd_2O_3	6.88	4.45	7.33	5.82	6.77	6.25
Sm_2O_3	2.97	3.08	2.06	2.80	2.67	2.71
Gd_2O_3	4.97	4.22	4.46	5.01	4.59	4.65
Tb_2O_3	0.33	0.35	0.32	0.25	0.38	0.33
Dy_2O_3	3.39	3.13	3.35	3.64	3.40	3.38
Er_2O_3	1.56	1.43	1.92	1.91	1.48	1.66
Yb_2O_3	0.46	0.55	0.70	0.76	0.64	0.62
Lu_2O_3	0.38	0.36	0.39	0.38	0.36	0.37
$H_2O_{calc.}$						1.60
F	0.00	0.10	0.04	0.12	0.05	0.06
Sum wt %	96.08	96.71	95.14	96.76	96.40	96.27
Si	4	4	4	4	4	4
B	4.86	4.58	4.83	3.77	4.60	4
Al	0.81	0.86	0.82	0.90	0.76	0.83
V	0.09	0.10	0.07	0.09	0.14	0.10
Be						0.04
Mg	0.00	0.10	0.00	0.11	0.00	0.04
Ca	1.51	1.23	1.55	1.26	1.51	1.41
Mn	1.66	1.90	1.67	1.89	1.68	1.76
Y	1.38	1.51	1.35	1.25	1.35	1.37
La	0.01	0.02	0.00	0.01	0.01	0.01
Ce	0.15	0.16	0.21	0.20	0.14	0.17
Pr	0.04	0.03	0.02	0.03	0.05	0.03
Nd	0.46	0.29	0.50	0.37	0.44	0.41
Sm	0.19	0.19	0.14	0.17	0.17	0.17
Gd	0.31	0.25	0.28	0.30	0.28	0.28
Tb	0.02	0.02	0.02	0.01	0.02	0.02
Dy	0.21	0.18	0.21	0.21	0.20	0.20
Er	0.09	0.08	0.11	0.11	0.09	0.10
Yb	0.03	0.03	0.04	0.04	0.04	0.03
Lu	0.02	0.02	0.02	0.02	0.02	0.02
OH						1.97
F	0.00	0.06	0.02	0.07	0.03	0.03
Σcat w/o B	10.99	10.98	11.01	10.97	10.90	11.01
Al + V	0.91	0.96	0.90	1.00	0.90	0.93
Me^{2+}	3.17	3.22	3.22	3.26	3.20	3.25
REE^{3+}	2.91	2.79	2.90	2.71	2.80	2.82
Mn/(Ca + Mn)	0.52	0.61	0.52	0.60	0.53	0.56

* Stoichiometric B_2O_3 in the "Mean" column and BeO from NanoSIMS.

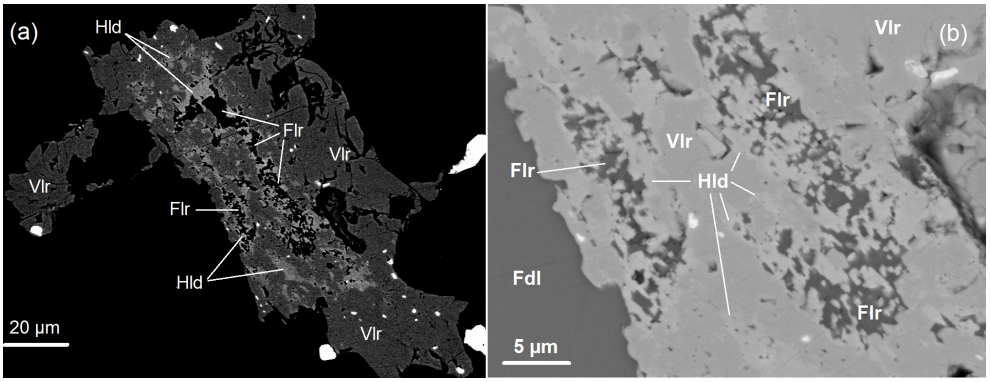

Figure 6. **(a)** High-contrast BSE picture showing a crystal of epidote (essentially a vanadoandrosite-(Ce)–vielleaureite-(Ce) solid solution (Vlr, dark grey)) hosting an intergrowth of hellandite (Hld, lighter grey) and fluorite (Flr, black). The hellandite seems to be shielding the fluorite. The black matrix is friedelite, rhodochrosite, and "Mn-humite". Cracks and holes in the right half of the epidote crystal are likely preparation artefacts. **(b)** Low-contrast close-up of panel **(a)**. Sample VAIN86.

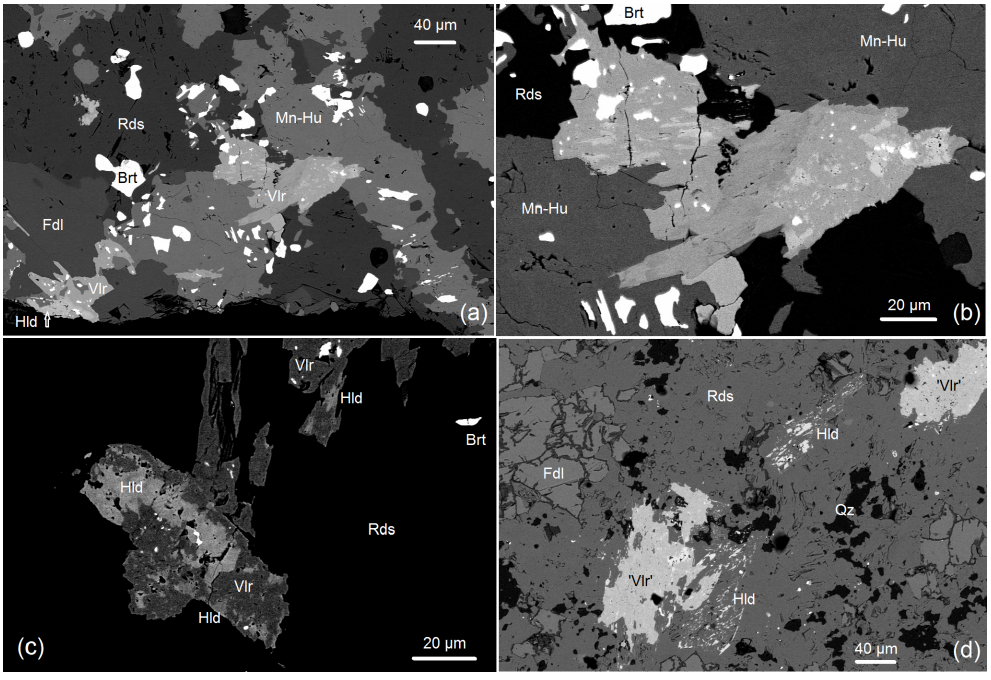

Figure 7. Textural relations of vielleaureite-(Ce) and hellandite. **(a)** Backscattered electron (BSE) image showing various relationships between hellandite (Hld, light grey) and vielleaureite-(Ce) (Vlr, medium grey) in a groundmass of rhodochrosite (Rds), a humite-group Mn mineral (Mn-Hu), friedelite (Fdl), and baryte (Brt). In the central group of epidote crystals, hellandite occurs as numerous oriented inclusions (details in panel **b**). In the crystal group of the lower-left corner at the thin-section edge, a larger hellandite crystal is partly overgrown by vielleaureite. To the left of this group, the tiny bright blobs lining the friedelite–Mn-humite interface are rare xenotime. Sample VAIN86. **(b)** Close-up of panel **(a)** showing the hellandite inclusions in the epidote phase, which are clearly oriented in the left epidote crystal. The various shades of grey of the epidote phase, all darker than that of hellandite, reflect compositional variations in the vielleaureite–vanadoandrosite solid solution, which may extend to other members (e.g. vanadoakasakaite). BSE image, sample VAIN86. **(c)** Another aspect of the relationships between vielleaureite and "hellandite" in a rhodochrosite groundmass. All bright speckles are baryte, except for the dumbbell-shaped hübnerite inclusion in the central hellandite area. BSE image, sample VAIN86. **(d)** Two "ghost" crystals of hellandite (Ca ∼ Mn) along with vielleaureite (actually a vielleaureite–vanadoandrosite solid solution) in a rhodochrosite–quartz–friedelite matrix. The lower ghost crystal is partly overgrown by the epidote phase. In this epidote aggregate, the larger hellandite inclusion (bright) contains tiny quartz inclusions (black). BSE image, sample VA2018-13.

tural formula $M3_2M4_2M2_2M1\ ^T\square_2Si_4B_4O_{22}(OH,F,O)_2$ (Oberti et al., 2002, where $^T\square$ stands for tetrahedral vacancy), these analyses show no evidence of vacancy in M sites (at variance with Miyawaki et al., 2015, but in line with Oberti et al., 2002, 2019). Whatever the nomenclature scheme (as addressed in the Supplement), they point to the existence of a new member in the hellandite group, the Mn^{2+} equivalent of hellandite-(Y). A formal definition has to be postponed until suitable material becomes available for further characterisation.

Compared to coexisting vielleaureite, which is free of yttrium, the complete partitioning of boron and yttrium in hellandite is a first-order feature (note the absence of tinzenite in these samples); besides, the allanite phase concentrates the light REEs (Ce, La, Nd), whereas the hellandite phase exploits the intermediate ones (Nd, Gd, Dy). It is therefore unlikely that hellandite, although closely associated with (and commonly included in) allanites, may have been significantly involved in their formation.

In any event, this new hellandite phase is the first member of the group with Mn^{2+} as the species-defining cation; its occurrence in metamorphosed Mn ores is also of a new type for hellandite-group minerals, which are typically reported from pegmatites, ejecta, or hydrothermal veins (but see Nikischer, 2002, for (Ca-rich) hellandite-(Y) or "ferrihellandite-(Y)" on rhodochrosite from Franklin, New Jersey).

Data availability. The crystallographic information files are available in the Supplement, together with analytical data.

Supplement. The supplement related to this article is available online at https://doi.org/10.5194/ejm-37-627-2025-supplement.

Author contributions. AR: sample collection, petrography, and EMP analysis. LB: single-crystal X-ray study, crystal-chemical considerations, and writing. PB: crystal-chemical considerations and writing. LR: NanoSIMS analysis. CC: petrography, EMP analysis, and writing.

Competing interests. At least one of the (co-)authors is a member of the editorial board of *European Journal of Mineralogy*. The peer-review process was guided by an independent editor, and the authors also have no other competing interests to declare.

Disclaimer. Publisher's note: Copernicus Publications remains neutral with regard to jurisdictional claims made in the text, published maps, institutional affiliations, or any other geographical representation in this paper. While Copernicus Publications makes every effort to include appropriate place names, the final responsibility lies with the authors.

Special issue statement. This article is part of the special issue "Celebrating the outstanding contribution of Paola Bonazzi to mineralogy". It is not associated with a conference.

Acknowledgements. The help of Michel Fialin and Nicolas Rividi (Camparis) with electron-microprobe analysis, of Damien Deldicque (ENS Paris) and Omar Boudouma (ISTeP) with electron microscopy, and of Julien Gasc (ENS Paris) with EBSD was much appreciated. Jean-Claude Boulliard (Collection des Minéraux de la Sorbonne) supplied the gem-quality samples used for NanoSIMS calibration. Christian Chopin is most grateful to Paola Bonazzi and Luca Bindi for involving him in the thrilling perbøeite adventure, which was his incentive for the present collaboration. The constructive critique of two anonymous referees is gratefully acknowledged.

Financial support. Alain Ragu was funded by the "Coup de pouce" programme of ISTeP, Sorbonne Université. Christian Chopin was funded by UMR8538, ENS-CNRS. The NanoSIMS facility at the Muséum national d'Histoire naturelle in Paris was established using funds from the CNRS, Région Ile de France, Ministère délégué à l'Enseignement supérieur et à la Recherche and the Muséum national d'Histoire naturelle.

Review statement. This paper was edited by Marco Pasero and reviewed by two anonymous referees.

References

Armbruster, T., Bonazzi, P., Akasaka, M., Bermanec V., Chopin, C., Gieré, R., Heuss-Assbichler, S., Liebscher, A., Menchetti, S., Pan, Y., and Pasero, M.: Recommended nomenclature of epidote-group minerals, Eur. J. Mineral., 18, 551–567, https://doi.org/10.1127/0935-1221/2006/0018-0551, 2006.

Biagioni, C., Bonazzi, P., Pasero, M., Zaccarini, F., Balestra, C., Bracco, R., and Ciriotti, M. E.: Manganiakasakaite-(La) and ferriakasakaite-(Ce), two new epidote supergroup minerals from Piedmont, Italy, Minerals, 9, 353, https://doi.org/10.3390/min9060353, 2019.

Bindi, L., Holtstam, D., Fantappié, G., Andersson, U. B., and Bonazzi, P.: Ferriperbøeite-(Ce), $[CaCe_3]_{\Sigma=4}[Fe^{3+}Al_2Fe^{2+}]_{\Sigma=4}[Si_2O_7][SiO_4]_3O(OH)_2$, a new member of the polysomatic epidote–törnebohmite series from the Nya Bastnäs Fe-Cu-REE deposit Sweden, Eur. J. Mineral., 30, 537–544, https://doi.org/10.1127/ejm/2018/0030-2717, 2018.

Bonazzi, P. and Menchetti, S.: Manganese in monoclinic members of the epidote group: Piemontite and related minerals, in: Epidotes, Rev. Mineral. Geochem., 56, 495–552, 2004.

Bonazzi, P., Menchetti, S., and Reinecke, T.: Solid solution between piemontite and androsite-(La), a new mineral of the epidote group from Andros island, Greece, Am. Mineral., 81, 735–743, 1996.

Bonazzi, P., Holtstam, D., and Bindi, L.: Gatelite-supergroup minerals: recommended nomenclature and review, Eur. J. Mineral., 31, 173-181, https://doi.org/10.1127/ejm/2019/0031-2809, 2019.

Brese, N. E. and O'Keeffe, M.: Bond-valence parameters for solids, Acta Cryst., B47, 192–197, 1991.

Brugger, J., Bonin, M., Schenk, K. J., Meisser, N., Berlepsch, P., and Ragu, A.: Description and crystal structure of nabiasite, $BaMn_9[(V,As)O_4]_6(OH)_2$, a new mineral from Central Pyrénées (France), Eur. J. Mineral., 11, 879–890, 1999.

Bruker AXS Inc.: APEX 3. Bruker Advanced X-ray Solutions, Madison, Wisconsin, USA. 2016.

Cenki-Tok, B., Ragu, A., Armbruster, T., Chopin, C., and Medenbach, O.: New Mn- and rare-earth-rich epidote-group minerals in metacherts: manganiandrosite-(Ce) and vanadoandrosite-(Ce), Eur. J. Mineral., 18, 569–582, https://doi.org/10.1127/0935-1221/2006/0018-0569, 2006.

Grew, E. S.: Tinzenite, a member of the axinite group with formula revised to $Ca_2Mn_4^{2+}Al_4[B_2Si_8O_{30}](OH)_2$, Eur. J. Mineral., 30, 177–182, https://doi.org/10.1127/ejm/2018/0030-2708, 2018.

Grew, E. S., Essene, E. J., Peacor, D. R., Su, S.-C., and Asami, M.: Dissakisite-(Ce), a new member of the epidote group and the Mg analogue of allanite-(Ce) from Antarctica, Am. Mineral., 76, 1990–1997, 1991.

Holtstam, D. and Andersson, U. B.: The REE minerals of the Bastnäs-type deposits, South-Central Sweden, Can. Mineral., 45, 1073–1114, 2007.

Holtstam, D., Kolitsch, U., and Andersson, U. B.: Västmanlandite-(Ce) – a new lanthanide- and F-bearing sorosilicate mineral from Västmanland, Sweden: description, crystal structure, and relation to gatelite-(Ce), Eur. J. Mineral., 17, 129–141, https://doi.org/10.1127/0935-1221/2005/0017-0129, 2005.

Lacroix, A.: Sur les minéraux des gisements manganésifères des Hautes Pyrénées, Bull. Soc. Fr. Minéral., 23, 251–255, https://doi.org/10.3406/bulmi.1900.2569, 1900.

Lemirre, B., Cochelin, B., Duchene, S., de Saint Blanquat, M., and Poujol, M.: Origin and duration of late orogenic magmatism in the foreland of the Variscan belt (Lesponne – Chiroulet - Néouvielle area, French Pyrénées), Lithos, 336–337, 183–201, 2019.

Levinson, A. A.: A system of nomenclature for rare-earth minerals, Am. Mineral., 51, 152–158, 1966.

Lienau, H.: Manganese silico-carbonates from Hautes-Pyrenees, Chem. Zeit., XXIII, 418–419, 1899 (in German).

Miyawaki, R., Yokoyama, K., Matsubara, S., Tsutsumi, Y., and Goto, A.: Uedaite-(Ce), a new member of the epidote group with Mn at the A site, from Shodoshima, Kagawa Prefecture, Japan, Eur. J. Mineral., 20, 261–269, https://doi.org/10.1127/0935-1221/2008/0020-1783, 2008.

Miyawaki, R., Moma, K., Yokoyama, K., Shigeoka, M., Matsubara, S., Ito, M., Nakai, I., and Kristiansen, R.: Mn-bearing hellandite-(Y) from the Heftetjern pegmatite, Tørdal, Norway, Can. Mineral., 53, 345–356, 2015.

Nagashima, M., Nishio-Hamane, D., Tomita, N., Minakawa, T., and Inaba, S.: Ferriakasakaite-(La) and ferriandrosite-(La): new epidote supergroup minerals from Ise, Mie Prefecture, Japan, Mineral. Mag., 79, 735–753, https://doi.org/10.1180/minmag.2015.079.3.16, 2015.

Nagashima, M., Nishio-Hamane, D., Ohnishi, M., and Harada, A.: Vanadoakasakaite-(Ce), IMA 2024-044, in: IMA Commission on New Minerals, Nomenclature and Classification (CNMNC) – Newsletter 82, Eur. J. Mineral., 36, 1005–1010, https://doi.org/10.5194/ejm-36-1005-2024, 2024.

Nikischer, T.: Hellandite, $(Ca,Y)_6(Al,Fe^{3+})_2Si_4B_4O_{20}(OH)_4$, Added to Franklin Species List, The Picking Table, 43, 7, https://www.fomsnj.org/PDF/PickingTable/PT43-1.pdf (last access: September 2025), 2002.

Oberti, R., Della Ventura, G., Ottolini, L., Hawthorne, F. C., and Bonazzi, P.: Re-definition, nomenclature and crystal-chemistry of the hellandite group, Am. Mineral., 87, 745–752, 2002.

Oberti, R., Langone, A., Boiocchi, M., Bernabè, E., and Hawthorne, F. C.: News from the hellandite group: the redefinition of mottanaite and ciprianiite and the new mineral description of ferrimottanaite-(Ce), the first Fe^{3+}-dominant hellandite, Eur. J. Mineral., 31, 799–806, https://doi.org/10.1127/ejm/2019/0031-2858, 2019.

Pautov, L. A., Khorov, P. V., Ignatenko, K. I., Sokolova, E. V., and Nadezhina, T. N.: Khristovite-(Ce), (Ca,REE)REE(Mg,Fe)AlMnSi_3O_{11}(OH)(F,O) – a new mineral of the epidote group. Zapiski Vserossijskogo Mineralogicheskogo Obshchestva, 122, 103–111, 1993.

Peacor, D. R. and Dunn, P. J.: Dollaseite-(Ce) (magnesium orthite redefined): structure refinement and implications for F + M^{2+} substitution in epidote-group minerals, Am. Mineral., 73, 838–842, 1988.

Pouchou, J. L. and Pichoir, F.: "PAP" $\varphi(\rho Z)$ procedure for improved quantitative microanalysis, in: Microbeam analysis – 1985, San Francisco Press, San Francisco, 104–160, 1985.

Ragu, A.: Pétrologie et minéralogie des minéralisations manganésées métamorphiques dans le Paléozoïque des Pyrénées Centrales. Mémoire des Sciences de la Terre, no. 90-15, Univ. P. et M. Curie, Paris, 328 pp., 1990.

Ragu, A.: Helvite from the French Pyrénées as evidence for granite-related hydrothermal activity, Can. Mineral., 32, 111–120, 1994.

Sheldrick, G. M.: Crystal structure refinement with SHELXL, Acta Cryst., C71, 3–8, 2015.

Števko, M., Myšlan, P., Biagioni, C., Mauro, D., and Mikuš, T.: Ferriandrosite-(Ce), a new member of the epidote supergroup from Betliar, Slovakia, Mineral. Mag., 87, 887–895, https://doi.org/10.1180/mgm.2023.62, 2023.

Taddei, A., Bonazzi, P., Förster, H.-J., Casey, P., Holtstam, D., Karlsson, A., and Bindi, L.: Multi-analytical characterization of an unusual epidote-supergroup mineral from Malmkärra, Sweden: Toward the new (OH)-analog of dollaseite-(Ce), Am. Mineral., 110, 594–602, https://doi.org/10.2138/am-2024-9438, 2025.